Journal of Sound and Vibration 327 (2009) 564–583

Contents lists available at ScienceDirect

Journal of Sound and Vibration

journal homepage: www.elsevier.com/locate/jsvi

Coupled vibration and parameter sensitivity analysis of rocking-mass vibrating gyroscopes

M. Ansari [a], E. Esmailzadeh [b,*], N. Jalili [c]

[a] Department of Mechanical and Mechatronics Engineering, University of Waterloo, Waterloo, Ontario, Canada N2L 3G1
[b] Faculty of Engineering and Applied Science, University of Ontario Institute of Technology Oshawa, Ontario, Canada L1 H 7K4
[c] Smart Structures and NEMS Laboratory, Department of Mechanical Engineering, Clemson University, Clemson, SC 29634-0921, USA

ARTICLE INFO

Article history:
Received 3 February 2009
Received in revised form
15 June 2009
Accepted 22 June 2009
Handling Editor: M.P. Cartmell
Available online 14 July 2009

ABSTRACT

Vibrating beam gyroscopes are widely used to measure the angle or the rate of rotation of many mechanical systems. The vibration and parameters sensitivity analyses of a specific type of vibrating beam gyroscope namely rocking-mass gyroscopes are presented in this paper. These types of gyroscopes by far have a better performance than the conventional single-beam gyroscopes. The system comprises of four slender beams attached to a rigid substrate, undergoing coupled flexural and torsional vibrations with a finite mass attached in the middle. Two of the beams carry piezoelectric patch actuators on top, while the other two possess piezoelectric patch sensors. Using extended Hamilton's principle, the resulting eight coupled partial differential equations of motion with their corresponding boundary conditions are derived. In spite of the need for a high computational power, the system is analysed in the frequency domain using an exact method and the closed-form characteristic equations for two cases of fixed and rotating base support are obtained. Furthermore, a detailed parameter sensitivity analysis is carried out to determine the effects of different parameters on the complex natural frequencies of the system. Results presented are valuable in the design of this type of gyroscope as the exact resonant conditions and the sensitivity of the system parameters play important roles in the dynamic performance of gyroscopes.

1. Introduction

Due to the wide range of the applications of the vibrating mass gyroscopes; they are being used in many navigational applications, namely, aerospace, marine and automobile industries. Hence, the detailed study of such systems has always been of great interest to engineers and researchers.

In most of these types of gyroscopes, the bending and torsional vibrations are coupled. The theory of coupled flexural–torsional vibrations for thin-walled beams was first developed by Timoshenko and Young [1]. The free flexural/torsional vibration of an Euler–Bernoulli beam with a rigid tip mass was studied by Oguamana [2]. He presented explicit expressions for the frequency equation, mode shapes and their orthogonality relationship and investigated the effects of different parameters on the fundamental frequencies of the system. Salarieh and Gorashi [3] continued his work, but used the Timoshenko beam theory. They studied the effects of the shear deformation and the rotary inertia on the free vibration response of a Timoshenko beam with a rigid tip mass. Gokdag and Kopmaz [4] extended the work of

* Corresponding author. Tel.: 1 905 721 8668x2600; fax: 1 905 721 3370.
E-mail address: ezadeh@uoit.ca (E. Esmailzadeh).

0022-460X/$ - see front matter © 2009 Elsevier Ltd. All rights reserved.
doi:10.1016/j.jsv.2009.06.021

Nomenclature

b	width of the beams
b_M	rocking-mass width
C_{ij} , C'_{ij}	elements of matrices
d_{31}	piezoelectric constant of actuators
E	elastic modulus of beams
E_p	elastic modulus of actuators
EI_b	flexural rigidity of the beams
EI_p	flexural rigidity of the actuator
G	beams shear modulus
GJ_b	torsional rigidity of the beams
GJ_p	torsional rigidity of the actuator
h_M	Rocking-mass height
i	$\sqrt{-1}$
I_{xb}	mass moment of inertia of the beams
I_{xp}	mass moment of inertia of the piezoelectric actuator
l	length of rocking-mass
l_1	start position of piezoelectric actuator
l_2	end position of piezoelectric actuator
L_i	length of ith beam
M	rocking-mass
M_P	piezoelectric actuator control moment
$Q_n(x)$	amplitude of torsion
$P_n(x)$	amplitude of bending
s_1	position of point P on beam 1
T	total kinetic energy of the system
t_b	beams thickness
t_p	piezoelectric layers thickness
T_{1b}	translational kinetic energy of the four beams due to the translational motion
T_{1M}	translational kinetic energy of the rocking-mass due to the translational motion
T_{2b}	translational kinetic energy of the four beams due to the rotational motion
T_{2M}	translational kinetic energy of the rocking-mass due to the rotational motion
V	total potential energy of the system
$v(t)$	voltage applied to actuators
w_i	bending of ith beam
W_{nc}	total non-conservative work done on the system
θ_i	torsion of ith beam
ρ_b	mass per unit length of the beams
ρ_p	mass per unit length of the piezoelectric actuator
ψ_i, θ_i	angle of rotations of ith beam
Ω_1	rotation about X_i-axis
Ω_2	rotation about Y_i-axis
Ω_3	rotation about Z_i-axis
ω	vibration frequency
ω_{ix}	angular velocity component of ith beam in x-direction
ω_{iy}	angular velocity component of ith beam in y-direction
ω_{iz}	angular velocity component of ith beam in z-direction

Oguamana [2] by studying the coupled flexural/torsional vibrations of a beam with either the tip or in the span mass attachments.

In a series of studies, Jalili and his research team [5–7] worked on the vibrating gyroscopic systems experiencing coupled flexural/torsional vibrations. Their first work was to develop a thorough modeling framework for vibrating gyroscopes subjected to general support motion by considering both the flexural and torsional vibrations [5]. In a subsequent work, they include a novel piezoelectric actuation for the vibrating beam gyroscope, which was modeled as an Euler-Bernoulli beam with a tip load subjected to the base rotation. They investigated the effect of the cross-axis in single beam vibratory gyroscopes [6], and also the influence of the substrate motion on the performance of the ring microgyroscopes [7].

Although vibrating beam gyroscopes are becoming the most widely used gyroscopes in many applications [6], but they possess a very important drawback, which produces the cross-coupling error in the measurements [6,8]. The vibrating beam gyroscope is typically used to measure the rotational rate around one of the axes. In practice, however, there are always some secondary rotations present in the system. These secondary base rotations can produce significant errors in the measurement of the gyroscope output (cross-axis error). The gyroscopic output increases significantly even for a small secondary rotation. This increased output could be interpreted as the gyroscope output due to the primary base rotation and can hence, develop errors in the measurement [6].

In spite of single beam gyroscopes, the rocking-mass gyroscope does not have those drawbacks, and can accurately measure the rate of rotation. Due to the complexities involved in the modelling and performance analysis of this kind of gyroscope, only few studies have been carried out in this area. The fabrication and design of a rocking-mass gyroscope was studied by Tang and Gutierrez [9], but the operating principle of the device was not fully discussed. Royle and Fox [10] presented an analysis of the mechanics of an oscillatory rate gyroscope that is actuated and sensed using thin piezoelectric actuators and sensors. A modeling framework for these systems, which forms the basis of this paper, is an extension to the work reported by Bhadbhade [11].

The present research undertakes the vibration analysis of a rocking-mass gyroscope, which comprises of a rotating rigid substrate and an assembly of four cantilever beams with a rigid mass attached to them in the middle, as shown in Fig. 1. The objective of the research is to develop a detailed mathematical modeling of the system. The governing equations of motion, using the extended Hamilton's principle, are derived. Since the closed-form solutions can serve as the benchmarks for validating the results obtained from either the numerical calculations or experimental results, the closed-form equations are developed for the frequency characteristic equations of the system for either a fixed supporting base or a rotating one. These exact equations are very important and useful, since their solutions would not only provide exact

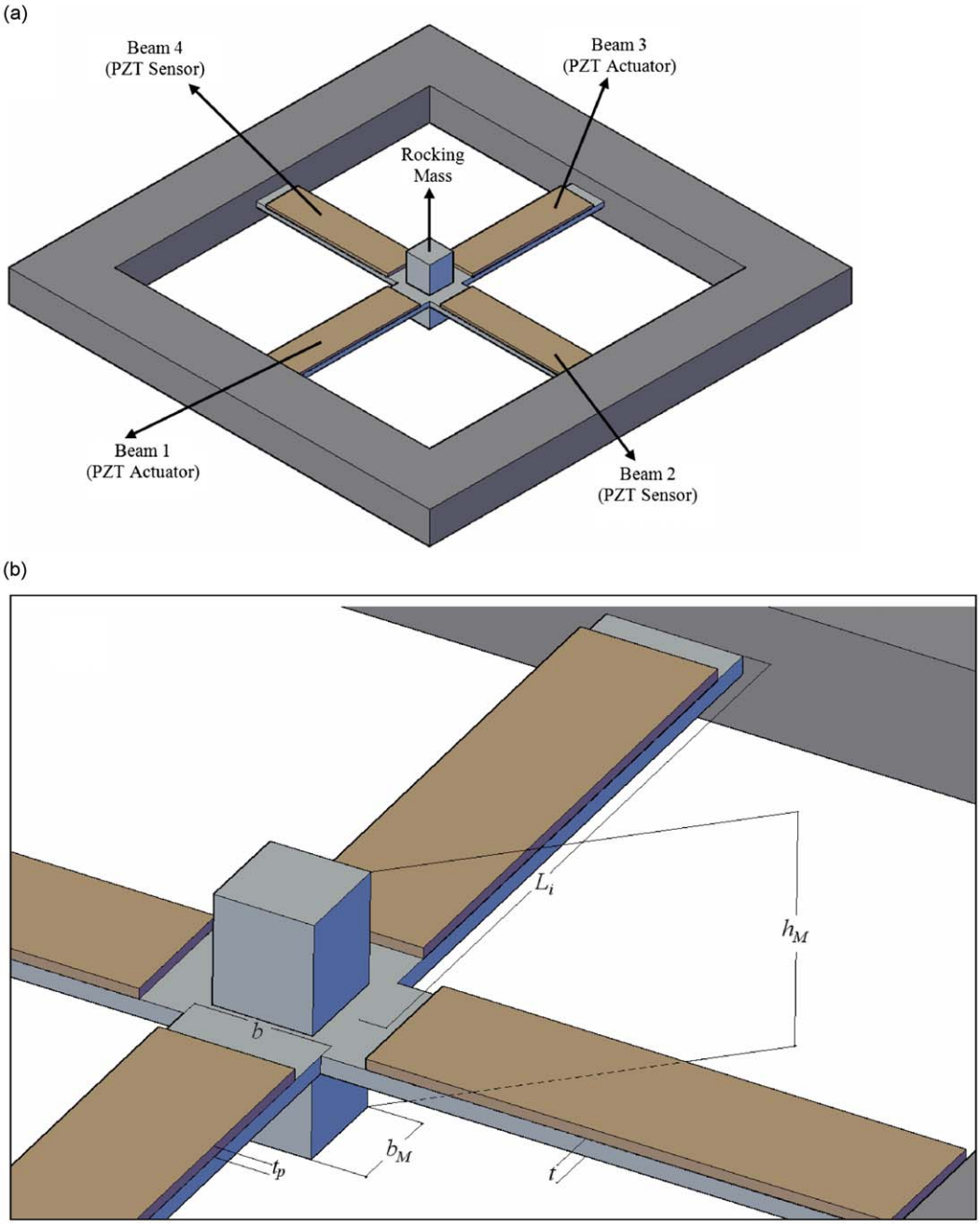

Fig. 1. Schematic of a rocking-mass gyroscope: (a) regular view; (b) zoomed view.

information about the system fundamental resonant frequencies and their corresponding mode shapes, but also they serve as the bases for the time-domain analyses.

In most of the works done so far, the time-domain analysis has been performed using the assumed mode method (AMM). In fact, instead of determining the exact complex natural frequencies and performing mode superposition method (MSM), in these works the mode shapes of the system have been assumed to have certain forms (AMM). In contrast, this paper offers a closed-form frequency equation and consequently exact fundamental frequencies which can serve as the basis of an accurate time domain analysis (MSM). Moreover, a thorough parametric sensitivity analysis is carried out to determine the effects of different parameters on the complex natural frequencies of the system.

2. Principle of operation

The rocking-mass gyroscope consists of four cantilever beams attached to a rocking-mass in the middle as shown in Fig. 1. In order to both induce and sense the vibrations in those beams, the piezoelectric actuators are attached to the beams 1 and 3, and the piezoelectric sensors are attached to the beams 2 and 4. The primary bending vibration is induced in the beams 1 and 3, by supplying a sinusoidal voltage to the piezoelectric patches on them. The rocking-mass will rotate due to the bending of beams 1 and 3, and produces a torsional vibration in the beams 2 and 4 as schematically illustrated in Fig. 2. In the presence of the base angular rotation about the vertical axis, a secondary rocking motion of the mass is induced due to the Coriolis force. Bending is induced in beams 2 and 4, as a result of the secondary rocking motion of the mass, as shown in Fig. 3. The amplitude of this bending vibration is proportional to the angular velocity of the base. This secondary bending vibration, which can be measured by piezoelectric sensors placed on beams 2 and 4, results into the angular velocity of the base.

Similar to the single beam gyroscope discussed in [11], the rocking-mass gyroscope utilizes the secondary induced vibrations to determine the rate of rotation. It is typically difficult to measure the secondary torsional vibrations for the single beam gyroscope, as their amplitude is relatively small. This drawback is overcome by the rocking-mass gyroscope, where the torsional vibrations produced in the two beams are transferred to the other two beams as the bending vibrations, which can easily be sensed by placing the sensors on the beams.

3. Mathematical modeling

The eight linear partial differential equations and their corresponding boundary conditions governing the flexural–torsional motions of the four beams of the gyroscope will be developed in this section, using the extended Hamilton's principle and the approach being presented in [6]. All the beams are assumed to follow the Euler–Bernoulli beam theory and accordingly, the effects of warping and shear deformation have been neglected. The beams are all considered to be identical and slender with the mass per unit length of ρ_b and the thickness of t_b and the Poisson's effect is also neglected. The four coordinate systems that are used to describe the kinematics of the rocking-mass gyroscope are illustrated in Fig. 4.

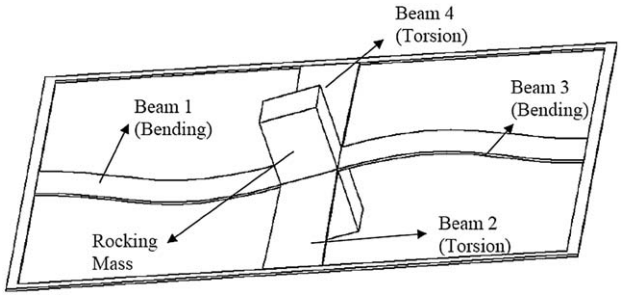

Fig. 2. Primary rocking motion of the mass [11].

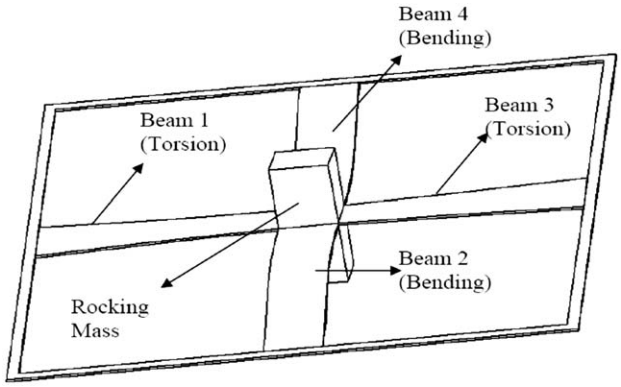

Fig. 3. Secondary rocking motion of the mass [11].

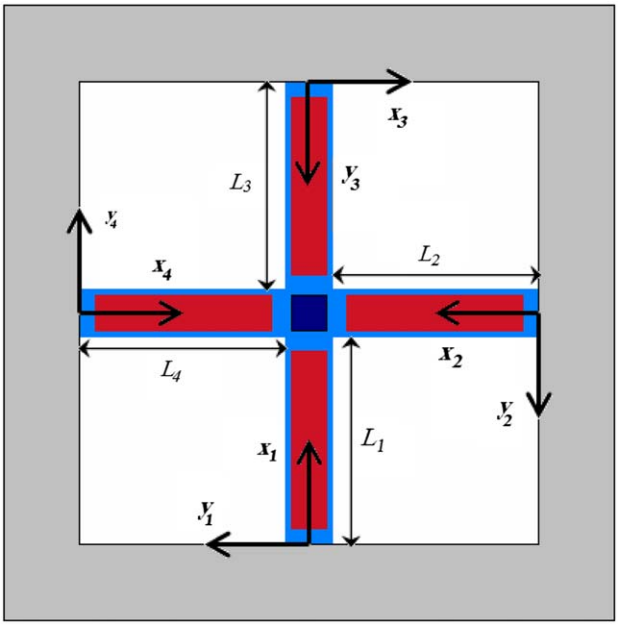

Fig. 4. Top view of the rocking-mass gyroscope with the coordinate systems.

The system is considered to have four identical beams of equal lengths denoted as $L_i(i = 1, 2, 3, 4)$, while the length of the rocking-mass is denoted by l. The bending and torsional deformations of the beams are represented by $w_i(i = 1, 2, 3, 4)$ and $\theta_i(i = 1, 2, 3, 4)$, respectively. In the derivation of the two coupled governing equations (one being for the bending and the other for torsion) for each of the four beams, the rocking-mass is considered to be attached to the first beam.

In order to apply the extended Hamilton's principle, the total translational kinetic energy, total rotational kinetic energy, total potential energy and the non-conservative work done on the system will be determined sequentially.

3.1. Translational motion

The total translational kinetic energy of the four beams can be determined in the following form [6,11]

$$T_{1b} = \frac{1}{2}\sum_{j=1}^{4}\left[\int_0^L \rho_b(f_j^2 + g_j^2 + h_j^2)\,\mathrm{d}x_j\right] \tag{1}$$

where

$$f_1 = 0, \quad f_2 = 0, \quad f_3 = 0, \quad f_4 = -w_4\Omega_2,$$

$$g_1 = -w_1\Omega_1 + s_1\Omega_3, \quad g_2 = s_2\Omega_3, \quad g_3 = w_3\Omega_1 + s_3\Omega_3, \quad g_4 = s_4\Omega_3,$$

$$h_1 = \frac{\partial w_1}{\partial t}, \quad h_2 = \frac{\partial w_2}{\partial t} - s_2\Omega_2, \quad h_3 = \frac{\partial w_3}{\partial t}, \quad h_4 = \frac{\partial w_4}{\partial t} + s_4\Omega_2. \tag{2}$$

Also, the translational kinetic energy of the rocking-mass can be expressed as [6]

$$T_{1M} = \frac{1}{2}M(f_M^2 + g_M^2 + h_M^2) \tag{3}$$

where

$$f_M = 0,$$

$$g_M = \Omega_3 L_1 - \Omega_1 w_{1L} + \Omega_3\frac{l}{2} - \Omega_1\frac{l}{2}\psi_{1L},$$

$$g_M = \Omega_3 L_1 - \Omega_1 w_{1L} + \Omega_3 \frac{l}{2} - \Omega_1 \frac{l}{2}\psi_{1L},$$

$$h_M = \frac{\partial w_{1L}}{\partial t} + \frac{l}{2}\frac{\partial \psi_{1L}}{\partial t} \tag{4}$$

and

$$w_{1L} \triangleq w_1(x_1, t)\big|_{x_1=L_1}, \quad \psi_{1L} \triangleq \frac{\partial w_1}{\partial x_1}\bigg|_{x_1=L_1} \tag{5}$$

3.2. Rotational motion

In order to describe the deformations of the beams and the rocking-mass from their original configuration, the Euler angles are considered. The two successive angles of rotation for each beam are considered and denoted as $\psi_i\,(i = 1, 2, 3, 4)$ and $\theta_i (i = 1, 2, 3, 4)$. Fig. 5 shows how these consecutive rotations take place. The system (X, Y, Z) is taken to (x′, Y, z′) by the first rotation ψ about *Y*-axis. Then, the second rotation θ, about x′, takes the new system to (x′, y, z), [11]. The angular velocity components of four beams, assuming small angles of bending and torsion and by ignoring the nonlinear terms, and the rocking-mass are expressed as

$$\omega_{1x} = \left(\frac{\partial\theta_1}{\partial t} + \Omega_1 - \Omega_3\psi_1\right), \quad \omega_{1y} = \left(\frac{\partial\psi_1}{\partial t} + \Omega_1\theta_1\psi_1 + \Omega_3\theta_1\right), \quad \omega_{1z} = (\Omega_1\psi_1 + \Omega_3)$$

$$\omega_{2x} = \left(\frac{\partial\theta_2}{\partial t} - \Omega_3\psi_2\right), \quad \omega_{2y} = \left(\frac{\partial\psi_2}{\partial t} + \Omega_2 + \Omega_3\theta_2\right), \quad \omega_{2z} = (\Omega_2\theta_2 + \Omega_3)$$

$$\omega_{3x} = \left(\frac{\partial\theta_3}{\partial t} + \Omega_1 - \Omega_3\psi_3\right), \quad \omega_{3y} = \left(\frac{\partial\psi_3}{\partial t} + \Omega_1\theta_3\psi_3 + \Omega_3\theta_3\right), \quad \omega_{3z} = (-\Omega_1\psi_3 + \Omega_3)$$

$$\omega_{4x} = \left(\frac{\partial\theta_4}{\partial t} - \Omega_3\psi_4\right), \quad \omega_{4y} = \left(\frac{\partial\psi_4}{\partial t} + \Omega_2 + \Omega_3\theta_4\right), \quad \omega_{4z} = (\Omega_2\theta_4 + \Omega_3) \tag{6}$$

where $\psi_i = \partial w_i/\partial x_i$, $i = 1, 2, 3, 4$.

Ignoring the rotary inertia terms for the beams, i.e., $I_{yb}\omega_y$ and $I_{zb}\omega_z$, one can write the rotational kinetic energy of the four beams as

$$T_{2b} = \sum_{j=1}^{4}\left[\int_0^{L_j}\left(\frac{1}{2}I_{xb}\omega_{jx}^2\right)\mathrm{d}x_j\right] \tag{7}$$

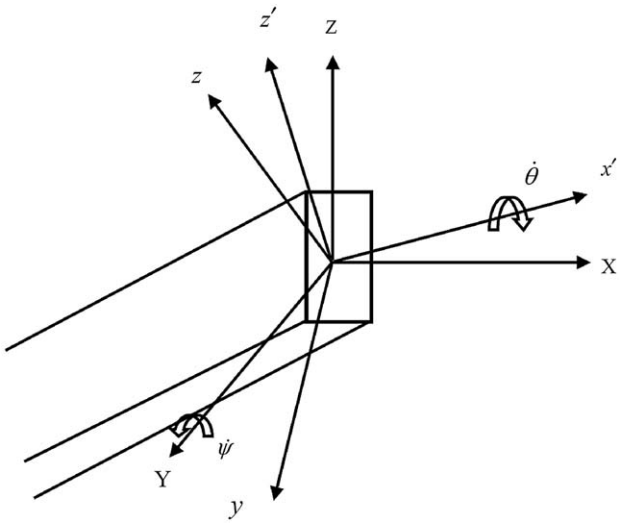

Fig. 5. Euler angle rotations [Fig. 5 of Ref. [6]].

Furthermore, the rotational kinetic energy of the rocking-mass is

$$T_{2M} = \frac{1}{2}(I_{xM}\omega_{1x}^2 + I_{yM}\omega_{1y}^2 + I_{zM}\omega_{1z}^2) \tag{8}$$

where the three terms I_{xb}, I_{yb}, I_{zb} and the three terms I_{xM}, I_{yM}, I_{zM} are the respective mass moments of inertia of the beams and those of the rocking-mass about the three X, Y and Z axes.

3.3. Equations of motion

The extended Hamilton's principle for a dynamic system is expressed as

$$\int_{t_1}^{t_2} \{\delta T - \delta V + \delta W_{nc}\}\, \mathrm{d}t = 0 \tag{9}$$

where T is the total kinetic energy of the system, V is the total potential energy and W_{nc} is the total non-conservative work done on the system.

Combining Eqs. (1), (3), (7) and (8), one can find the total kinetic energy of the system as

$$T = \frac{1}{2}\sum_{j=1}^{4}[\int_0^{L_j} \{\rho(x_j)[f_j^2 + g_j^2 + h_j^2] + I_x(x_j)\omega_{jx}^2\}\mathrm{d}x_j] + \frac{1}{2}M(f_M^2 + g_M^2 + h_M^2) + \frac{1}{2}(I_{xM}\omega_{1x}^2 + I_{yM}\omega_{1y}^2 + I_{zM}\omega_{1z}^2) \tag{10}$$

where

$$\rho(x_1) = (\rho_b + S(x_1)\rho_p), \quad \rho(x_2) = \rho_b$$

$$\rho(x_3) = (\rho_b + S(x_2)\rho_p), \quad \rho(x_4) = (\rho_b + S(x_4)\rho_p)$$

$$I_x(x_1) = (I_{xb} + S(x_1)I_{xp}), \quad I_x(x_2) = I_{xb}$$

$$I_x(x_3) = (I_{xb} + S(x_3)I_{xp}), \quad I_x(x_4) = (I_{xb} + S(x_4)I_{xp}) \tag{11}$$

in which, ρ_p and I_{xp} are the mass per unit length and the mass moment of inertia of the piezoelectric actuator, respectively. $S(x)$ is used to define the finite length of the piezoelectric and is given as

$$S(x) = H(x - l_1) - H(x - l_2) \tag{12}$$

where l_1 and l_2 are the respective starting and end positions of the piezoelectric actuator on the beam 1, and H represents the Heaviside function.

Since there is no vertical motion for the rocking-mass, the total potential energy of the system consists of only the four beams, which can be stated as

$$V = \frac{1}{2}\sum_{j=1}^{4}\left[\int_0^{L_j}\left\{EI(x_j)\left(\frac{\partial^2 w_j}{\partial x_j^2}\right)^2 + GJ(x_j)\left(\frac{\partial \theta_j}{\partial x_j}\right)^2\right\}\mathrm{d}x_j\right] \tag{13}$$

where EI_b and EI_p are the respective flexural rigidities of the beam and the actuator, and GJ_b and GJ_p are the torsional rigidities of the beam and the actuator, respectively.

$$I(x_1) = (I_{xb} + S(x_1)I_{xp}), \quad I(x_2) = I_{xb}$$

$$I(x_3) = (I_{xb} + S(x_3)I_{xp}), \quad I(x_4) = (I_{xb} + S(x_4)I_{xp})$$

$$J(x_1) = (J_{xb} + S(x_1)J_{xp}), \quad J(x_2) = J_{xb}$$

$$J(x_3) = (J_{xb} + S(x_3)J_{xp}), \quad J(x_4) = (J_{xb} + S(x_4)J_{xp}) \tag{14}$$

In the Hamilton's approach, the piezoelectric actuator control moment can be expressed in accordance with the following virtual work expression [6,12,13].

$$\delta W_{nc} = \int_0^{L_1} \frac{\partial^2 M_p}{\partial x_1^2}\delta w_1\, \mathrm{d}x_1 + \int_0^{L_1} \frac{\partial^2 M_p}{\partial x_3^2}\delta w_3\, \mathrm{d}x_3 \tag{15}$$

where

$$M_p = -\frac{1}{2}bE_p d_{31}(t_b + t_p)v(t)S(x) = M_{p0}v(t)S(x) \tag{16}$$

for each beams. In Eq. (16), b is the width of the beams 1 and 3, E_p and d_{31} are the respective elastic modulus and piezoelectric constant of the actuators placed on the two beams, and $v(t)$ is the voltage applied to the actuators.

In order to derive the governing equations of motion and the corresponding boundary conditions, one should take the variations of Eqs. (10) and (13) and substitute the results along with Eq. (15) into the Hamilton's principle (Eq. (9)). These will result in

$$\rho(x_1)\left(\frac{\partial^2 w_1}{\partial t^2}-w_1\Omega_1^2+s_1\Omega_1\Omega_3\right)-I_x(x_1)\Omega_3\left(\frac{\partial^2\theta_1}{\partial t\partial x_1}+\Omega_3\frac{\partial^2 w_1}{\partial x_1^2}\right)+\frac{\partial^2}{\partial x_1^2}\left(EI(x_1)\left(\frac{\partial^2 w_1}{\partial x_1^2}\right)\right)=\frac{\partial^2 M_P}{\partial x_1^2} \tag{17}$$

$$I_x(x_1)\left(\frac{\partial^2\theta_1}{\partial t^2}+\Omega_3\frac{\partial^2 w_1}{\partial t\partial x_1}\right)-\frac{\partial}{\partial x_1}\left(GJ(x_1)\left(\frac{\partial\theta_1}{\partial x_1}\right)\right)=0 \tag{18}$$

$$\rho(x_2)\left(\frac{\partial^2 w_2}{\partial t^2}-w_2\Omega_2^2\right)-I_x(x_2)\Omega_3\left(\frac{\partial^2\theta_2}{\partial t\partial x_2}+\Omega_3\frac{\partial^2 w_2}{\partial x_2^2}\right)+\partial\frac{\partial^2}{\partial x_2^2}\left(EI(x_2)\left(\frac{\partial^2 w_2}{\partial x_2^2}\right)\right)=0 \tag{19}$$

$$I_x(x_2)\left(\frac{\partial^2\theta_2}{\partial t^2}+\Omega_3\frac{\partial^2 w_2}{\partial t\partial x_2}\right)-\frac{\partial}{\partial x_2}\left(GJ(x_2)\left(\frac{\partial\theta_2}{\partial x_2}\right)\right)=0 \tag{20}$$

$$\rho(x_3)\left(\frac{\partial^2 w_3}{\partial t^2}-w_3\Omega_1^2+s_3\Omega_1\Omega_3\right)-I_x(x_3)\Omega_3\left(\frac{\partial^2\theta_3}{\partial t\partial x_3}+\Omega_3\frac{\partial^2 w_3}{\partial x_3^2}\right)+\frac{\partial^2}{\partial x_3^2}\left(EI(x_3)\left(\frac{\partial^2 w_3}{\partial x_3^2}\right)\right)=\frac{\partial^2 M_P}{\partial x_3^2} \tag{21}$$

$$I_x(x_3)\left(\frac{\partial^2\theta_3}{\partial t^2}+\Omega_3\frac{\partial^2 w_3}{\partial t\partial x_3}\right)-\frac{\partial}{\partial x_3}\left(GJ(x_3)\left(\frac{\partial\theta_3}{\partial x_3}\right)\right)=0 \tag{22}$$

$$\rho(x_4)\left(\frac{\partial^2 w_4}{\partial t^2}-w_4\Omega_2^2\right)-I_x(x_4)\Omega_3\left(\frac{\partial^2\theta_4}{\partial t\partial x_4}+\Omega_3\frac{\partial^2 w_4}{\partial x_4^2}\right)+\frac{\partial^2}{\partial x_4^2}\left(EI(x_4)\left(\frac{\partial^2 w_4}{\partial x_4^2}\right)\right)=0 \tag{23}$$

$$I_x(x_4)\left(\frac{\partial^2\theta_4}{\partial t^2}+\Omega_3\frac{\partial^2 w_4}{\partial t\partial x_4}\right)-\frac{\partial}{\partial x_4}\left(GJ(x_4)\left(\frac{\partial\theta_4}{\partial x_4}\right)\right)=0 \tag{24}$$

and the boundary conditions are given as

$$w_j\big|_{x_j=0}=0,\ \frac{\partial w_j}{\partial x_j}\bigg|_{x_j=0}=0,\ \theta_j\big|_{x_j=0}=0;\quad j=1,2,3,4 \tag{25}$$

$$\begin{aligned}&I_x(x_1)\Omega_3\left(\frac{\partial\theta_1}{\partial t}+\Omega_1-\Omega_3\frac{\partial w_1}{\partial x_1}\right)\bigg|_{x_1=L_1}+M\Omega_1\left(-\Omega_3\left(L_1+\frac{l}{2}\right)+\Omega_1\left(w_1+\frac{l}{2}\frac{\partial w_1}{\partial x_1}\right)\right)\bigg|_{x_1=L_1}\\&-M\left(\frac{\partial^2 w_1}{\partial t^2}+\frac{l}{2}\frac{\partial^3 w_1}{\partial t^2\partial x_1}\right)\bigg|_{x_1=L_1}+EI(x_1)\left(\frac{\partial^3 w_1}{\partial x_1^3}\right)\bigg|_{x_1=L_1}=0\end{aligned} \tag{26}$$

$$\begin{aligned}&M\left(-\Omega_1\frac{l}{2}-\frac{l}{2}\left(\frac{\partial^2 w_1}{\partial t^2}+\frac{l}{2}\frac{\partial^3 w_1}{\partial t^2\partial x_1}\right)\bigg|_{x_1=L_1}\right)\\&+I_{xM}\Omega_3\left(\frac{\partial\theta_1}{\partial t}+\Omega_1-\Omega_3\frac{\partial w_1}{\partial x_1}\right)\bigg|_{x_1=L_1}\\&-I_{yM}\left(\frac{\partial^3 w_1}{\partial t^2\partial x_1}+\Omega_1\frac{\partial(\theta_1\psi_1)}{\partial t}+\Omega_3\frac{\partial\theta_1}{\partial t}\right)\bigg|_{x_1=L_1}\\&+I_{yM}\Omega_1\theta_{1L}\left(\frac{\partial^2 w_1}{\partial t\partial x_1}+\Omega_1\theta_1\frac{\partial w_1}{\partial x_1}+\Omega_3\theta_1\right)\bigg|_{x_1=L_1}\\&-I_{zM}\Omega_1\left(\Omega_1\frac{\partial w_1}{\partial x_1}+\Omega_3\right)\bigg|_{x_1=L_1}-EI(x_1)\left(\frac{\partial^2 w_1}{\partial x_1^2}\right)\bigg|_{x_1=L_1}=0\end{aligned} \tag{27}$$

$$
\begin{aligned}
&- I_{zM}\left(\frac{\partial^2\theta_1}{\partial t^2} - \Omega_3\frac{\partial^2 w_1}{\partial t\partial x_1}\right)\Big|_{x_1=L_1}\\
&+ I_{yM}\left(\frac{\partial^2 w_1}{\partial t\partial x_1} + \Omega_1\theta_1\frac{\partial w_1}{\partial x_1} + \Omega_3\theta_1\right)\Big|_{x_1=L_1}\Omega_1\frac{\partial w_1}{\partial x_1}\Big|_{x_1=L_1}\\
&- I_{yM}\Omega_3\left(\frac{\partial^2 w_1}{\partial t\partial x_1} + \Omega_1\theta_1\frac{\partial w_1}{\partial x_1} + \Omega_3\theta_1\right)\Big|_{x_1=L_1} - GJ(x_1)\left(\frac{\partial w_1}{\partial x_1}\right)\Big|_{x_1=L_1} = 0
\end{aligned}
\tag{28}
$$

Eqs. (26)–(28) have been written for the first beam; however, the vibrations of the tip of the other beams are related to these equations. Therefore, the bending and the torsional displacements of beams 2, 3 and 4 can be written in terms of the first beam, which forms the rest of the boundary conditions.

$$\delta w_{2L} = \delta w_{1L} + \frac{l}{2}\delta(\psi_{1L}), \quad \delta(\psi_{2L}) = \delta\theta_{1L}, \quad \delta\theta_{2L} = \delta(\psi_{1L}), \tag{29}$$

$$\delta w_{3L} = \delta w_{1L} + l\delta(\psi_{1L}), \quad \delta(\psi_{3L}) = -\delta(\psi_{1L}), \quad \delta\theta_{3L} = -\delta\theta_{1L}, \tag{30}$$

$$\delta w_{4L} = \delta w_{1L} + \frac{l}{2}\delta(\psi_{1L}), \quad \delta(\psi_{4L}) = -\delta\theta_{1L}, \quad \delta\theta_{4L} = -\delta(\psi_{1L}). \tag{31}$$

where

$$w_{jL} = w_j(x_j,t)\Big|_{x_j=L_j}; \quad j = 1,2,3,4 \tag{32}$$

$$\theta_{jL} = \theta_j(x_j,t)\Big|_{x_j=L_j}; \quad j = 1,2,3,4 \tag{33}$$

$$\psi_{jL} = \frac{\partial w_j}{\partial x_j}\Big|_{x_j=L_j}; \quad j = 1,2,3,4 \tag{34}$$

and $\delta(\cdot)$ represents the variation of the corresponding terms.

The governing equations of motion, given by Eqs. (17)–(24), indicate that for every beam, the two equations are coupled through the base rotation velocity, Ω_3. Furthermore, each of the beams experiences a coupled flexural–torsional vibration due to the gyroscopic terms such as $I_x\Omega_3(\partial^2\theta_i/\partial t\partial x_i)$ and $I_x\Omega_3(\partial^2 w_i/\partial t\partial x_i)$ present in the equations of motion. Consequently, in the absence of the base rotation velocity, the two equations of each beam will be decoupled. The second type of coupling is expressed through the continuity equations, i.e., Eqs. (29)–(31). The continuity equations represent the relationship between the flexural and torsional vibrations of beams 2, 3 and 4 in terms of the corresponding vibrations of beam 1. As discussed before, the bending of beams 1 and 3 induces a rocking motion in the mass. In the presence of the base rotation, this induced motion produces flexural vibrations in beams 2 and 4 and the torsional vibrations in beams 1 and 3. Since all the beams are connected to each other through the rocking-mass, the flexural and torsional deflections of each beam are also dependent on each other.

For simplification, Ω_1 is ignored for further analyses. Furthermore, the same cross-sectional areas and materials are considered for each beam. This means that instead of non-uniform material distribution dented by ρ_{xi} in the ith beam, the material is uniformly distributed over it and can be denoted by ρ_{xi}. Therefore, the governing equations of motion can be reduced to

$$\rho_j\frac{\partial^2 w_j}{\partial t^2} - I_{xj}\Omega_3\left(\frac{\partial^2\theta_j}{\partial t\partial x_j} + \Omega_3\frac{\partial^2 w_j}{\partial x_j^2}\right) + EI_j\frac{\partial^4 w_j}{\partial x_j^4} = \frac{\partial^2 M_P}{\partial x_j^2}; \quad j = 1,3 \tag{35}$$

$$I_{xj}\left(\frac{\partial^2\theta_j}{\partial t^2} + \Omega_3\frac{\partial^2 w_j}{\partial t\partial x_j}\right) - GJ_j\frac{\partial^2\theta_j}{\partial x_j^2} = 0; \quad j = 1,2,3,4 \tag{36}$$

$$\rho_j\left(\frac{\partial^2 w_j}{\partial t^2} - w_j\Omega_2^2\right) - I_{xj}\Omega_3\left(\frac{\partial^2\theta_j}{\partial t\partial x_j} + \Omega_3\frac{\partial^2 w_j}{\partial x_j^2}\right) + EI_j\frac{\partial^4 w_j}{\partial x_j^4} = 0; \quad j = 2,4 \tag{37}$$

4. Frequency analysis

An exact method is utilized here to develop the frequency equation. The solutions of the equations of motion, assuming harmonic motion with frequency ω, can be represented in the following form

$$\begin{cases} w_n(x,t) = P_n(x)e^{i\omega t} \\ \theta_n(x,t) = Q_n(x)e^{i\omega t} \end{cases} \quad n = 1,2,3,4 \tag{38}$$

where $P_n(x)$ and $Q_n(x)$ are the amplitudes of the sinusoidally varying bending and torsional displacements, respectively.

Substituting Eq. (38) into Eqs. (35)–(37) yields the following set of equations, which are only functions of the spatial variables x_1 through x_4.

$$\rho_j\omega^2 P_j(x_j) + iI_{xj}\omega\Omega_3 Q_j'(x_j) + I_{xj}\Omega_3^2 P_j''(x_j) - EI_j P_j^{IV}(x_j) = 0; \quad j = 1,3 \tag{39}$$

$$I_{xj}\omega^2 Q_j(x_j) - iI_{xj}\omega\Omega_3 P_j'(x_j) + GJ_j Q_j''(x_j) = 0; \quad j = 1,2,3,4 \tag{40}$$

$$\rho_j(\omega^2 + \Omega_2^2)P_j(x_j) + iI_{xj}\omega\Omega_3 Q_j'(x_j) + I_{xj}\Omega_3^2 P_j''(x_j) - EI_j P_j^{IV}(x_j) = 0; \quad j = 2,4 \tag{41}$$

The new set of boundary conditions can be expressed as

$$P_j(0) = 0, \quad P_j'(0) = 0, \quad Q_j(0) = 0; \quad j = 1,2,3,4 \tag{42}$$

$$M\omega^2 P_1(L_1) + (0.5Ml\omega^2 - I_{x1}\Omega_3^2)P_1'(L_1) + EI_1 P_1'''(L_1) + iI_{x1}\omega\Omega_3 Q_1(L_1) = 0 \tag{43}$$

$$2Ml\omega^2 P_1(L_1) + (Ml^2\omega^2 - 4I_{xM}\Omega_3^2 + 4I_{yM}\omega^2)P_1'(L_1) - 4EI_1 P_1''(L_1) + [(4i\omega\Omega_3)(I_{xM} - I_{yM})]Q_1(L_1) = 0 \tag{44}$$

$$(I_{xM}\omega^2 - I_{yM}\Omega_3^2)Q_1(L_1) - GJ_1 Q_1'(L_1) + [(i\omega\Omega_3)(I_{xM} - I_{yM})]P_1'(L_1) = 0 \tag{45}$$

$$P_2(L_2) = P_1(L_1) + 0.5lP_1'(L_1); \quad P_2'(L_2) = Q_1(L_1); \quad Q_2(L_2) = P_1'(L_1) \tag{46}$$

$$P_3(L_3) = P_1(L_1) + lP_1'(L_1); \quad P_3'(L_3) = -P_1'(L_1); \quad Q_3(L_3) = -Q_1(L_1) \tag{47}$$

$$P_4(L_4) = P_1(L_1) + 0.5lP_1'(L_1); \quad P_4'(L_4) = -Q_1(L_1); \quad Q_4(L_4) = -P_1'(L_1) \tag{48}$$

where $i = \sqrt{-1}$and $()'$represents the derivative with respect to the spatial variable x.

The solutions of Eqs. (39)–(41), in the absence of the primary base rotation,Ω_3, can be expressed in the following form. Detailed solutions are given in Appendix A.

$$P_j(x_j) = \sum_{n=6j-5}^{6j-2} A_n e^{s_n x_j}; \quad Q_j(x_j) = \sum_{n=6j-1}^{6j} A_n e^{s_n x_j}; \quad j = 1,2,3,4 \tag{49}$$

However, when there is a primary base rotation in the system, the solutions of Eqs. (39)–(41) will be stated as (refer to the detailed solutions presented in Appendix A)

$$P_1(x_1) = \sum_{n=1}^{24} A_n e^{s_n x_1}; \quad Q_1(x_1) = \sum_{n=1}^{24} A_n \alpha_n e^{s_n x_1} \tag{50}$$

Substituting either Eq. (49) or (50) into Eqs. (42)–(48) yields the following system of equations. The detailed derivations of these equations are presented in Appendix B.

$$C_{24\times 24} \times A_{24\times 1} = 0 \tag{51}$$

In order for this equation to have a nontrivial solution, the determinant of the matrix C should be equal to zero. This condition gives the closed-form characteristic (frequency) equation as

$$\det([C]_{24\times 24}) = 0 \tag{52}$$

5. Parameter sensitivity analysis

In this section, the sensitivity of the complex natural frequencies of the system to different parameters involved, such as the base rotation, the value of the mass and the length of the mass are studied. Since there is no explicit damping element in the system at hand, the complex frequencies result from the characteristics of the system, i.e., the coupled vibration and

Table 1
Physical parameters of the system.

Parameter	Notation	Value
Beams length (m)	L_1 , L_2 , L_3 , L_4	0.0508
Beams moment of inertia (kg.m^2)	I_{x1} , I_{x2} , I_{x3} , I_{x4}	2.0624×10^{-7}
Beams moment of inertia (m^4)	I_1 , I_2 , I_3 , I_4	2.2916×10^{-8}
Beams moment of inertia (m^4)	J_1 , J_2 , J_3 , J_4	2.2915×10^{-7}
Mass per unit length (kg/m)	ρ_1 , ρ_2 , ρ_3 , ρ_4	3960
Beams elastic modulus (GPa)	E	70
Beams shear modulus (GPa)	G	30
Rocking-mass length (m)	l	0.0175
Rocking-mass width (m)	b_M	0.0175
Rocking-mass height (m)	h_M	0.0175
Base rotation (rad/s)	Ω_3	0–50
Secondary rotation (rad/s)	Ω_2	0–50

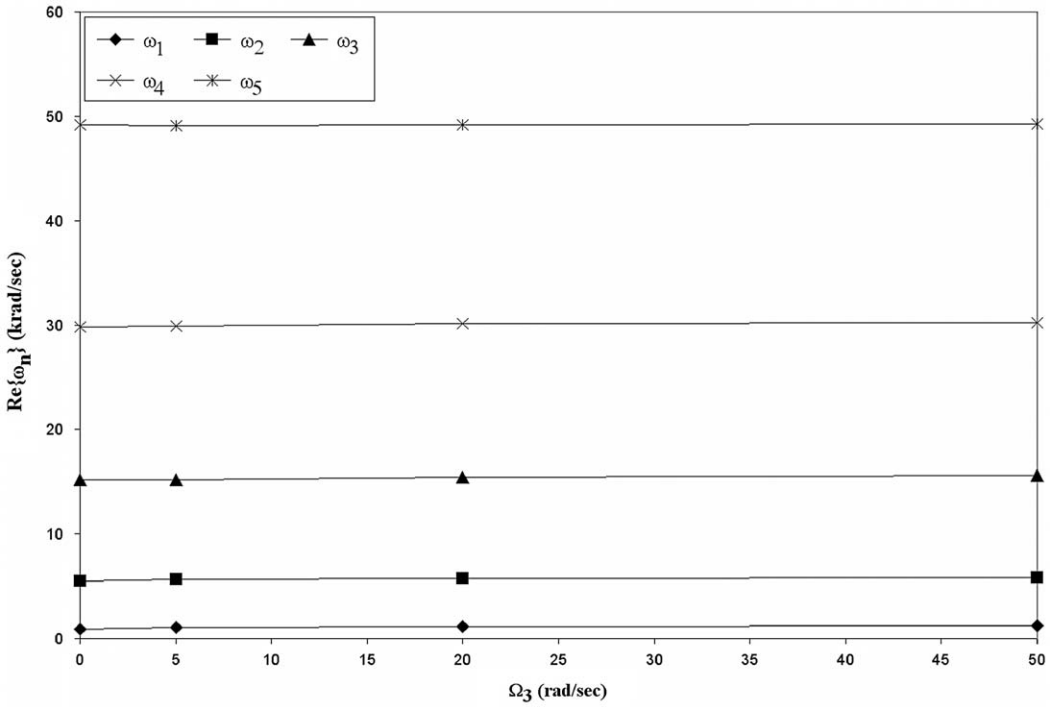

Fig. 6. Variations of the real part of complex natural frequencies with base rotation, $\Omega_2 = 0$.

Coriolis effects. The real part of the complex natural frequencies gives the frequency of vibration and the imaginary part refers to the rate of decay.

In order to perform the numerical analysis, a typical system with the arbitrary values of the parameters, given in Table 1, has been chosen. All the numerical analyses are performed in Maple©. The secant method [14] has been utilized to find the roots of the characteristic frequency equation.

5.1. Sensitivity to the primary base rotation, Ω_3

In this section, the primary base rotation is varied to determine its effects on the first five complex natural frequencies of the system. It should be noted that the model predicts all the infinite numbers of the natural frequencies of the system and its prediction is not just limited to five. Since the closed-form frequency equation is a very lengthy, its solution needs very high computational power. Therefore, only the first five natural frequencies have been presented here. Moreover, the first

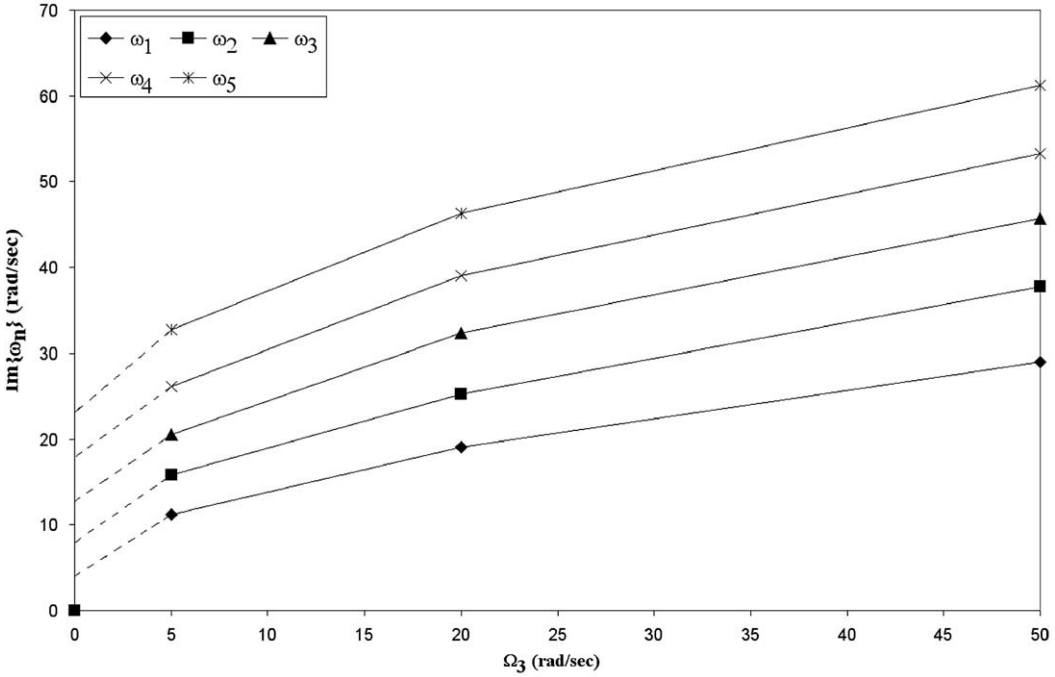

Fig. 7. Variations of the imaginary part of complex natural frequencies with base rotation, $\Omega_2 = 0$.

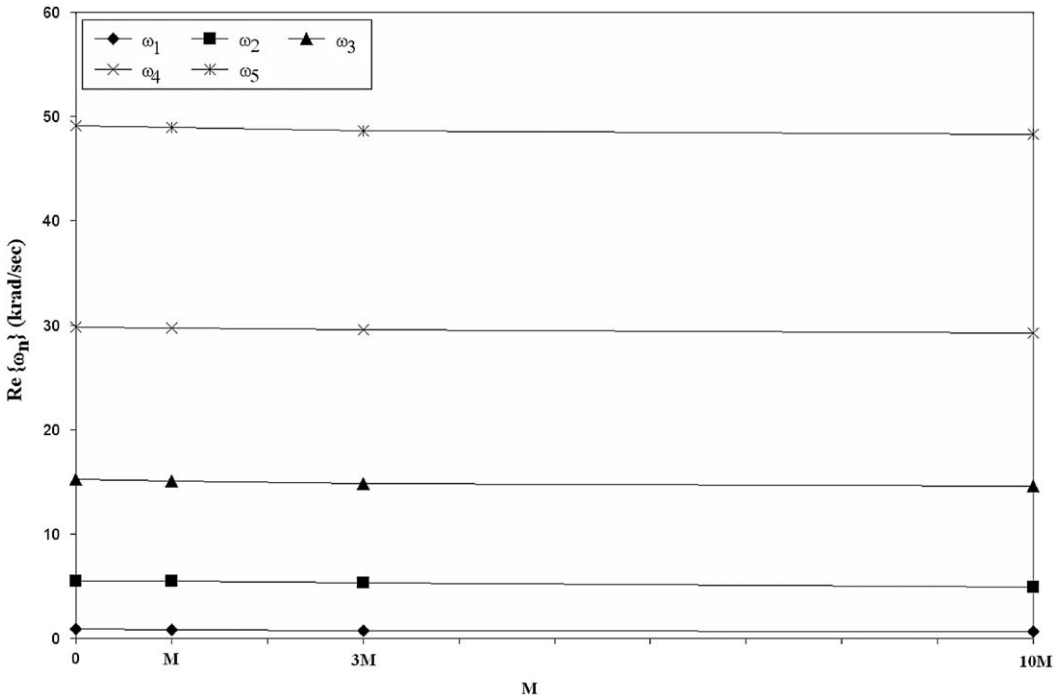

Fig. 8. Variations of the real part of complex natural frequencies with the value of the mass for $\Omega_3 = 20$.

few natural frequencies of the system are more important than the higher ones. The variations of the real and imaginary parts of the natural frequencies with the base rotation are illustrated in Figs 6 and 7, respectively.

The first point to highlight here is that in the absence of the base rotation, all the natural frequencies only have real values; however, when the beam undergoes base rotation, they will have both real and imaginary parts. As mentioned

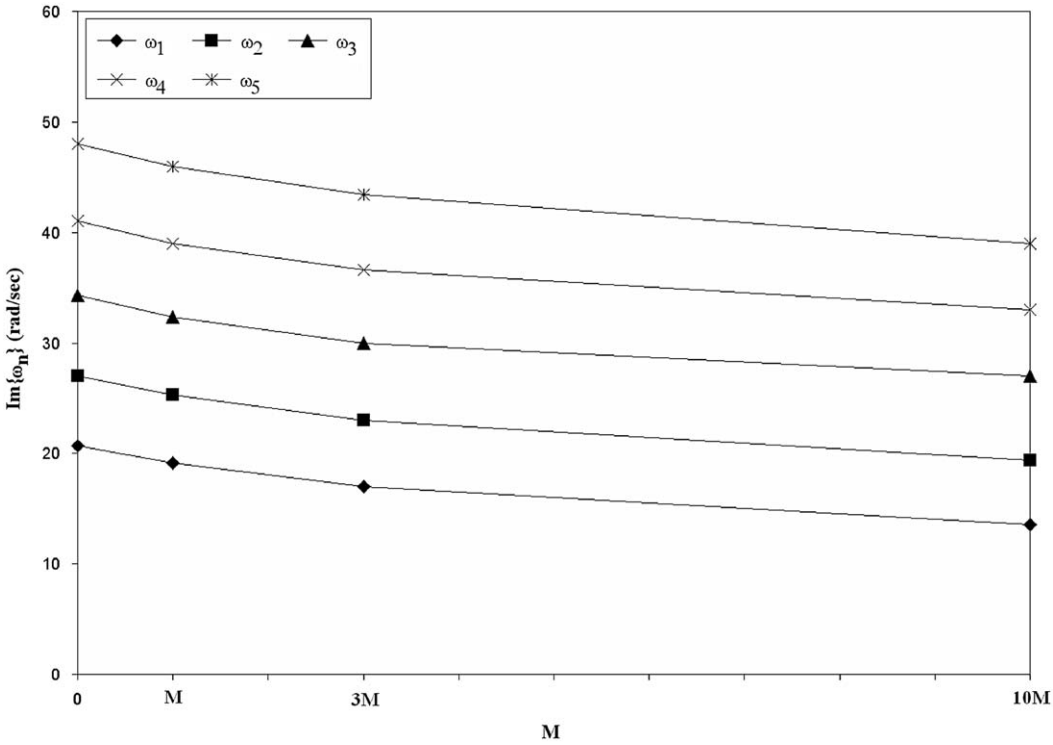

Fig. 9. Variations of the imaginary part of complex natural frequencies with mass for $\Omega_3 = 20$.

before, in the systems with explicit damping elements, the real part of the complex natural frequency is referred to damped natural frequency and its complex part gives the rate of decay. In analogy, one can conclude that the base rotation produces some sort of damping effects in the system.

From the jump phenomenon illustrated in Fig. 7 (after zero), it is clear that even having a very small base rotation can produce a considerable value of the imaginary part in the complex natural frequencies. Also, it can be concluded that the increase in the base rotation would increase the real and the imaginary parts of the complex frequencies. In other words, the higher the base rotation, the stiffer the system will become.

It can be seen from Figs. 6 and 7 that the imaginary part of the frequency increases faster than the real part. The reason for it is that in every pair of the equations for each beam, the value of EI_n is much larger than that of $I_{xn}\Omega_3$ and the $I_{xn}\Omega_3^2$ terms, and moreover, the value of GJ_n is much larger than I_{xn} and $I_{xn}\Omega_3$ terms. As a result, the effect of Ω_3 on the real parts of the frequencies is masked for small rotations.

5.2. Sensitivity to rocking mass

This part reveals how the value of the mass and its dimension can affect the complex natural frequencies of the system.

5.2.1. Sensitivity to mass M

The value of the mass of the rocking-mass M is varied from zero to 10 times its base value, and then the variations of the real and the imaginary parts of the complex natural frequencies are investigated as depicted in Figs 8 and 9, respectively.

It can be concluded that as the mass of the rocking-mass increases, both the real and the imaginary parts of the complex natural frequencies of the system will decrease. Since the base value of the mass is very small in this study, the effects of the value of the mass are more sensible at higher values.

5.2.2. Sensitivity to rocking-mass length, l

The variations of the real and the imaginary parts of the complex natural frequencies with the mass length being varied from zero to twice of its base value are illustrated in Fig. 10 and 11, respectively.

It can be seen that the increase in the length of the mass would result into higher values of the real and the imaginary parts of the complex natural frequencies.

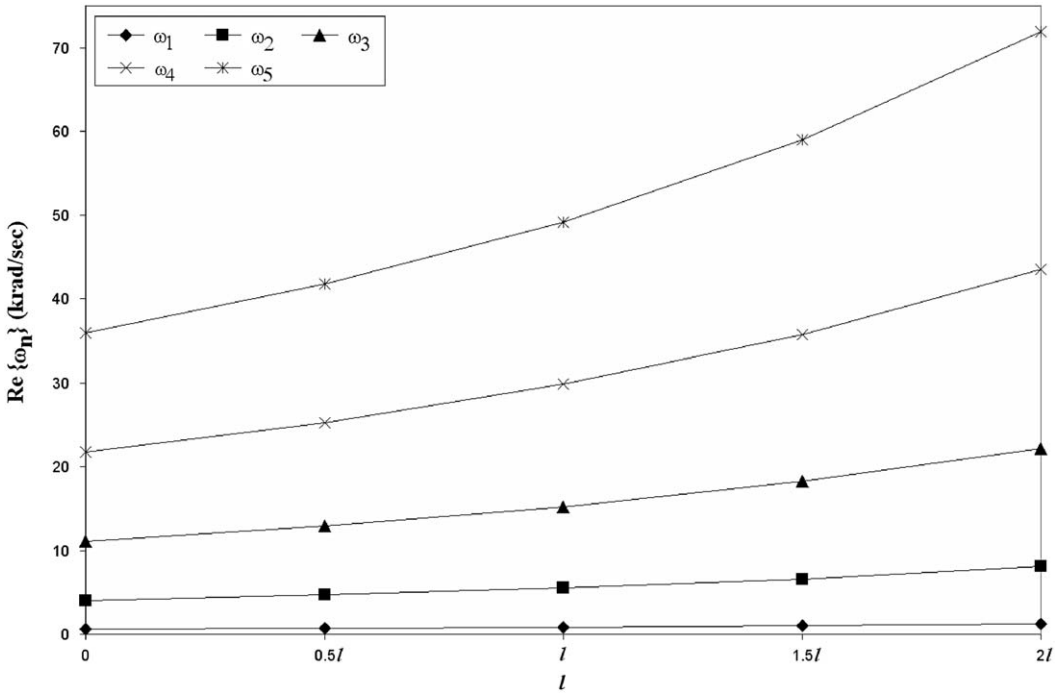

Fig. 10. Variations of the real part of complex natural frequencies with length of the rocking-mass for $\Omega_3 = 20$.

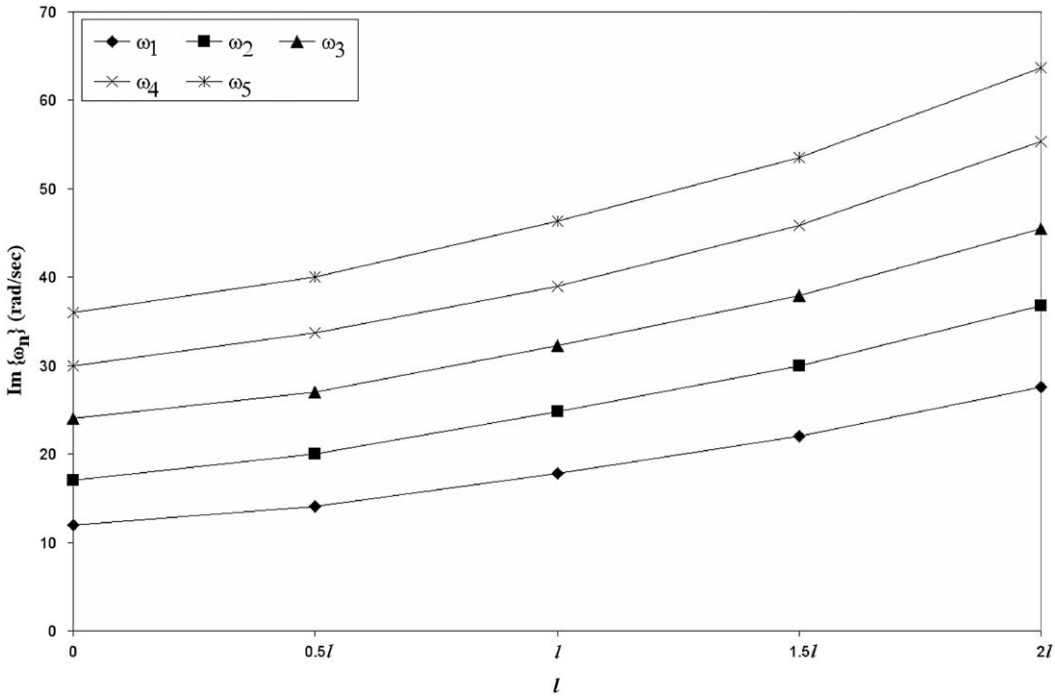

Fig. 11. Variations of the imaginary part of complex natural frequencies with length of the rocking-mass for $\Omega_3 = 20$.

5.3. *Sensitivity to secondary base rotation, Ω_2*

In this part, the effects of the secondary base rotation on the complex natural frequencies of the system are studied. The variations of the real and imaginary parts of the first five complex natural frequencies with the changes of Ω_2 from zero to 50 rad/s are presented in Figs. 12 and 13, respectively.

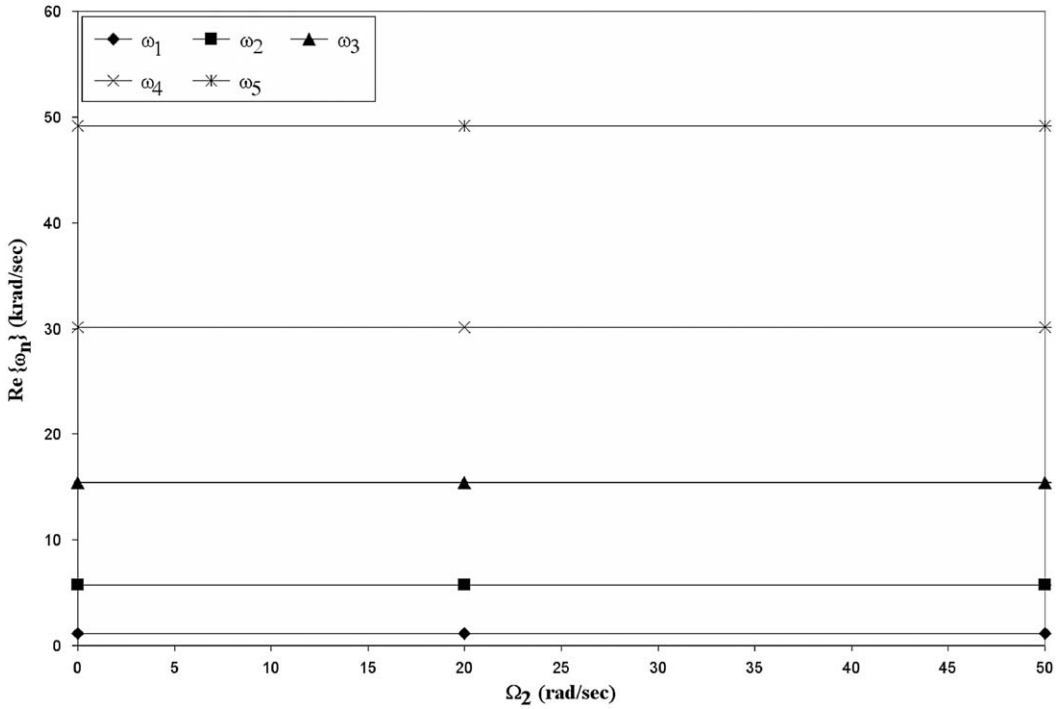

Fig. 12. Variations of the real part of complex natural frequencies with Ω_2 for $\Omega_3 = 20$.

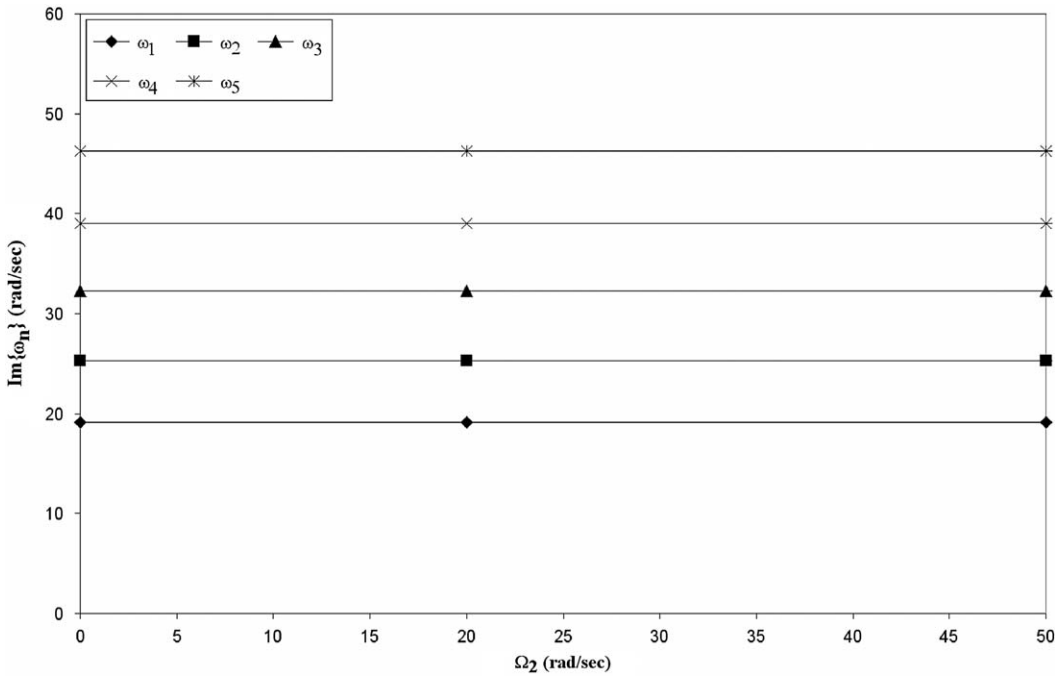

Fig. 13. Variations of the imaginary part of complex natural frequencies with Ω_2 for $\Omega_3 = 20$.

It can be seen that there are no significant frequency variations when Ω_2 is varied from zero to 50 rad/s. It should be noted that higher values of Ω_2 have also been considered, however, no significant differences were observed. This indicates that the secondary base rotation has almost no effect on the complex natural frequencies of the system. This is a valuable finding and is a significant result of the unique configuration of the rocking-mass gyroscope.

6. Conclusions

The traditional single beam gyroscopes often encounter with cross-axis error in their measurements as the secondary rotation is always available in reality. The rocking-mass gyroscope, consists of four elastic beams with the piezoelectric sensors and actuators and a mass attached to them in the middle, provides a better performance. However, due to the complexities of the analysis of such a system, this area had remained intact. Along this line of reasoning, the vibration of a rocking-mass gyroscope was studied in this paper. The eight coupled partial differential equations as well as the twenty four boundary conditions were derived for the system using the extended Hamilton's principle. The closed-form characteristic equation of the system was obtained for the two different cases of the fixed supporting base and the rotating one. The parameter sensitivity analysis was also performed on the system and the effects of the primary and the secondary base rotations as well as the value and the length of the rocking-mass on the complex natural frequencies of the system were determined. Results obtained demonstrate that the increase in the primary base rotation would increase the real and the imaginary parts of the frequencies; however, the secondary base rotation has almost no effect on them. In addition, an increase in rocking-mass will decrease the frequencies, while also increasing the rocking-mass length causes a higher values of the real and the imaginary parts of the complex natural frequencies.

Appendix A. Detailed solutions of Eqs. (39–41)

The solutions of Eqs. (39) and (40), when $j=1$, are considered to have the following forms

$$P_1(x_1) = A\mathrm{e}^{sx_1} \tag{A.1}$$

$$Q_1(x_1) = B\mathrm{e}^{sx_1} \tag{A.2}$$

where "s" is an expression in terms of the system parameters and ω, and can be found through Eq. (A.7).

Substituting Eqs. (A.1) and (A.2) into Eqs. (39) and (40), when $j=1$, yields

$$\rho_1\omega^2 A + iI_{x1}\omega\Omega_3 sB + I_{x1}\Omega_3^2 s^2 A - EI_1 s^4 A = 0 \tag{A.3}$$

$$I_{x1}\omega^2 B - iI_{x1}\omega\Omega_3 sA + GJ_1 s^2 B = 0 \tag{A.4}$$

From (A.3) and (A.4), it can be found that

$$\frac{A}{B} = \frac{-iI_{x1}\omega\Omega_3 s}{\rho_1\omega^2 + I_{x1}\Omega_3^2 s^2 - EI_1 s^4} \tag{A.5}$$

$$\frac{A}{B} = \frac{I_{x1}\omega^2 + GJ_1 s^2}{iI_{x1}\omega\Omega_3 s} \tag{A.6}$$

Comparing (A.5) and (A.6), one could conclude that

$$(\rho_1\omega^2 + I_{x1}\Omega_3^2 s^2 - EI_1 s^4)(I_{x1}\omega^2 + GJ_1 s^2) + (iI_{x1}\omega\Omega_3 s)^2 = 0 \Rightarrow s_n, n = 1,2,\ldots,6 \tag{A.7}$$

from which, the characteristic roots $s_n, n = 1,2,\ldots,6$ can be obtained.

Therefore, the solutions of Eqs. (39) and (40), when $j=1$, can be written in the following form

$$P_1(x_1) = \sum_{n=1}^{6} A_n \mathrm{e}^{s_n x_1} \tag{A.8}$$

$$Q_1(x_1) = \sum_{n=1}^{6} A_n \alpha_n \mathrm{e}^{s_n x_1} \tag{A.9}$$

where

$$\alpha_n = \frac{iI_{x1}\omega\Omega_3 s_n}{I_{x1}\omega^2 + GJ_1 s_n^2}, \quad n = 1,2,\ldots,6 \tag{A.10}$$

Following the same approach for each pairs of Eq. (39)–(41), one can determine a couple of equations similar to Eqs. (A.7) and (A.10) for each pair in the following form

$$[\rho_2(\omega^2+\Omega_2^2) + I_{x2}\Omega_3^2 s^2 - EI_2 s^4][I_{x2}\omega^2 + GJ_2 s^2] + (iI_{x2}\omega\Omega_3 s)^2 = 0 \Rightarrow s_n\alpha_n = \frac{iI_{x2}\omega\Omega_3 s}{I_{x2}\omega^2 + GJ_2 s^2}, \quad n = 7,\ldots,12 \tag{A.11}$$

$$(\rho_3\omega^2 + I_{x3}\Omega_3^2 s^2 - EI_3 s^4)(I_{x3}\omega^2 + GJ_3 s^2) + (iI_{x3}\omega\Omega_3 s)^2 = 0 \Rightarrow s_n\alpha_n = \frac{iI_{x3}\omega\Omega_3 s_n}{I_{x3}\omega^2 + GJ_3 s_n^2}, \quad n = 13,\ldots,18 \tag{A.12}$$

$$[\rho_4(\omega^2+\Omega_2^2)+I_{x4}\Omega_3^2 s^2-EI_4 s^4][I_{x4}\omega^2+GJ_4 s^2]+(iI_{x4}\omega\Omega_3 s)^2=0\Rightarrow s_n\alpha_n=\frac{iI_{x4}\omega\Omega_3 s}{I_{x4}\omega^2+GJ_4 s^2},\quad n=19,\ldots,24 \tag{A.13}$$

Therefore, the solutions of Eqs. (39)–(41), in the presence of the primary base rotation of Ω_3, can be written in the form of Eq. (50).

In the absence of the primary base rotation, each pairs of Eqs. (39)–(41) will be decoupled. Following the same approach as stated here, one can determine the eight equations whose roots ares$_n$, used in Eq. (49).

$$\left.\begin{array}{c}\rho_j\omega^2-EI_j s^4=0\Rightarrow s_n, n=6j-5,\ldots,6j-2\\ I_{xj}\omega^2+GJ_j s^2=0\Rightarrow s_n, n=6j-1,6j\end{array}\right\}\quad j=1,2,3,4 \tag{A.14}$$

Appendix B. Closed-form frequency equation

Substituting Eq. (49) into the Eqs (42)–(48) yields the following system of equations in the matrix form.

$$\begin{bmatrix} C'_1 & C'_2 & C'_3 & C'_4\\ C'_5 & C'_6 & C'_7 & C'_8\\ C'_9 & C'_{10} & C'_{11} & C'_{12}\\ C'_{13} & C'_{14} & C'_{15} & C'_{16}\end{bmatrix}\begin{bmatrix} A'_1\\ A'_2\\ A'_3\\ A'_4\end{bmatrix}=\begin{bmatrix} Z_1\\ Z_2\\ Z_3\\ Z_4\end{bmatrix} \tag{B.1}$$

where

$$Z_1=Z_2=Z_3=Z_4=0_{(6\times1)} \tag{B.2}$$

$$A'_m=\begin{bmatrix} A_m\\ A_{m+1}\\ A_{m+2}\\ A_{m+3}\\ A_{m+4}\\ A_{m+5}\end{bmatrix},\quad m=1,\ldots,4 \tag{B.3}$$

$$C'_1=\begin{bmatrix} 1 & 1 & 1 & 1 & 0 & 0\\ s_1 & s_2 & s_3 & s_4 & 0 & 0\\ 0 & 0 & 0 & 0 & s_5 & s_6\\ 0 & 0 & 0 & 0 & 0 & 0\\ 0 & 0 & 0 & 0 & 0 & 0\\ 0 & 0 & 0 & 0 & 0 & 0\end{bmatrix};\quad C'_2=\begin{bmatrix} 0 & 0 & 0 & 0 & 0 & 0\\ 0 & 0 & 0 & 0 & 0 & 0\\ 0 & 0 & 0 & 0 & 0 & 0\\ 1 & 1 & 1 & 1 & 0 & 0\\ s_7 & s_8 & s_9 & s_{10} & 0 & 0\\ 0 & 0 & 0 & 0 & s_{11} & s_{12}\end{bmatrix} \tag{B.4}$$

$$C'_7=\begin{bmatrix} 1 & 1 & 1 & 1 & 0 & 0\\ s_{13} & s_{14} & s_{15} & s_{16} & 0 & 0\\ 0 & 0 & 0 & 0 & s_{17} & s_{18}\\ 0 & 0 & 0 & 0 & 0 & 0\\ 0 & 0 & 0 & 0 & 0 & 0\\ 0 & 0 & 0 & 0 & 0 & 0\end{bmatrix};\quad C'_8=\begin{bmatrix} 0 & 0 & 0 & 0 & 0 & 0\\ 0 & 0 & 0 & 0 & 0 & 0\\ 0 & 0 & 0 & 0 & 0 & 0\\ 1 & 1 & 1 & 1 & 0 & 0\\ s_{19} & s_{20} & s_{21} & s_{22} & 0 & 0\\ 0 & 0 & 0 & 0 & s_{23} & s_{24}\end{bmatrix} \tag{B.5}$$

$$C'_9=\begin{bmatrix} c'_{131} & c'_{132} & c'_{133} & c'_{134} & c'_{135} & c'_{136}\\ c'_{141} & c'_{142} & c'_{143} & c'_{144} & c'_{145} & c'_{146}\\ 0 & 0 & 0 & 0 & 0 & 0\\ c'_{161} & c'_{162} & c'_{163} & c'_{164} & c'_{165} & c'_{166}\\ 0 & 0 & 0 & 0 & 0 & 0\\ c'_{181} & c'_{182} & c'_{183} & c'_{184} & c'_{185} & c'_{186}\end{bmatrix};\quad C'_{13}=\begin{bmatrix} c'_{191} & c'_{192} & c'_{193} & c'_{194} & c'_{195} & c'_{196}\\ c'_{201} & c'_{202} & c'_{203} & c'_{204} & c'_{205} & c'_{206}\\ 0 & 0 & 0 & 0 & 0 & 0\\ c'_{221} & c'_{222} & c'_{223} & c'_{224} & c'_{225} & c'_{226}\\ 0 & 0 & 0 & 0 & 0 & 0\\ c'_{241} & c'_{242} & c'_{243} & c'_{244} & c'_{245} & c'_{246}\end{bmatrix} \tag{B.6}$$

$$C'_{10}=\begin{bmatrix}0&0&0&0&0&0\\0&0&0&0&0&0\\0&0&0&0&0&0\\c'_{167}&c'_{168}&c'_{169}&c'_{1610}&c'_{1611}&c'_{1612}\\c'_{177}&c'_{178}&c'_{179}&c'_{1710}&c'_{1711}&c'_{1712}\\0&0&0&0&0&0\end{bmatrix}$$
$$C'_3=C'_4=C'_5=C'_6=C'_{11}=C'_{12}=C'_{14}=\mathbf{0}_{(6\times6)} \tag{B.7}$$

$$C'_{15}=\begin{bmatrix}c'_{1913}&c'_{1914}&c'_{1915}&c'_{1916}&c'_{1917}&c'_{1918}\\c'_{2013}&c'_{2014}&c'_{2015}&c'_{2016}&c'_{2017}&c'_{2018}\\0&0&0&0&0&0\\0&0&0&0&0&0\\0&0&0&0&0&0\\0&0&0&0&0&0\end{bmatrix};\quad C'_{16}=\begin{bmatrix}0&0&0&0&0&0\\0&0&0&0&0&0\\0&0&0&0&0&0\\c'_{2219}&c'_{2220}&c'_{2221}&c'_{2222}&c'_{2223}&c'_{2224}\\c'_{2319}&c'_{2320}&c'_{2321}&c'_{2322}&c'_{2323}&c'_{2324}\\0&0&0&0&0&0\end{bmatrix} \tag{B.8}$$

where

$$\begin{gathered}n=1,\ldots,6\\ C'_{13n}=[M\omega^2+0.5.Mls_n\omega^2+EI_1s_n^3]e^{s_nL_1}\\ C'_{14n}=[2Ml\omega^2+(Ml^2\omega^2+4I_{yM}\omega^2)s_n-4EI_1s_n^2]e^{s_nL_1}\\ C'_{16n}=-[1+0.5ls_n]e^{s_nL_1};\quad C'_{18n}=-s_ne^{s_nL_1};\quad C'_{19n}=-[1+ls_n]e^{s_nL_1}\\ C'_{20n}=s_ne^{s_nL_1};\quad C'_{22n}=-[1+0.5ls_n]e^{s_nL_1};\quad C'_{24n}=s_ne^{s_nL_1}\end{gathered} \tag{B.9}$$

$$n=7,\ldots,12\rightarrow c'_{16n}=e^{s_nL_2};\quad c'_{17n}=s_ne^{s_nL_2} \tag{B.10}$$

$$n=13,\ldots,18\rightarrow c'_{19n}=e^{s_nL_3};\quad c'_{20n}=s_ne^{s_nL_3} \tag{B.11}$$

$$n=19,\ldots,24\rightarrow c'_{22n}=e^{s_nL_4};\quad c_{23n}=s_ne^{s_nL_4} \tag{B.12}$$

where s_n are found from Eq. (A.14).

In this case, the characteristic equation would become

$$\det\begin{bmatrix}C'_1&C'_2&C'_3&C'_4\\C'_5&C'_6&C'_7&C'_8\\C'_9&C'_{10}&C'_{11}&C'_{12}\\C'_{13}&C'_{14}&C'_{15}&C'_{16}\end{bmatrix}=0 \tag{B.13}$$

Substituting Eq. (50) into Eq. (42)–(48) yields the following system of equations.

$$\begin{bmatrix}C_1&C_2&C_3&C_4\\C_5&C_6&C_7&C_8\\C_9&C_{10}&C_{11}&C_{12}\\C_{13}&C_{14}&C_{15}&C_{16}\end{bmatrix}\begin{bmatrix}A'_1\\A'_2\\A'_3\\A'_4\end{bmatrix}=\begin{bmatrix}Z_1\\Z_2\\Z_3\\Z_4\end{bmatrix} \tag{B.14}$$

where

$$C_1=\begin{bmatrix}1&1&1&1&1&1\\s_1&s_2&s_3&s_4&s_4&s_5\\\alpha_1&\alpha_2&\alpha_3&\alpha_4&\alpha_4&\alpha_5\\0&0&0&0&0&0\\0&0&0&0&0&0\\0&0&0&0&0&0\end{bmatrix};\quad C_2=\begin{bmatrix}0&0&0&0&0&0\\0&0&0&0&0&0\\0&0&0&0&0&0\\1&1&1&1&1&1\\s_7&s_8&s_9&s_{10}&s_{11}&s_{12}\\\alpha_7&\alpha_8&\alpha_9&\alpha_{10}&\alpha_{11}&\alpha_{12}\end{bmatrix} \tag{B.15}$$

$$C_7=\begin{bmatrix}1&1&1&1&1&1\\ s_{13}&s_{14}&s_{15}&s_{16}&s_{17}&s_{18}\\ \alpha_{13}&\alpha_{14}&\alpha_{15}&\alpha_{16}&\alpha_{17}&\alpha_{18}\\ 0&0&0&0&0&0\\ 0&0&0&0&0&0\\ 0&0&0&0&0&0\end{bmatrix};\quad C_8=\begin{bmatrix}0&0&0&0&0&0\\ 0&0&0&0&0&0\\ 0&0&0&0&0&0\\ 1&1&1&1&1&1\\ s_{19}&s_{20}&s_{21}&s_{22}&s_{23}&s_{24}\\ \alpha_{19}&\alpha_{20}&\alpha_{21}&\alpha_{22}&\alpha_{23}&\alpha_{24}\end{bmatrix} \tag{B.16}$$

$$C_9=\begin{bmatrix}c_{131}&c_{132}&c_{133}&c_{134}&c_{135}&c_{136}\\ c_{141}&c_{142}&c_{143}&c_{144}&c_{145}&c_{146}\\ c_{151}&c_{152}&c_{153}&c_{154}&c_{155}&c_{156}\\ c_{161}&c_{162}&c_{163}&c_{164}&c_{165}&c_{166}\\ c_{171}&c_{172}&c_{173}&c_{174}&c_{175}&c_{176}\\ c_{181}&c_{182}&c_{183}&c_{184}&c_{185}&c_{186}\end{bmatrix};\quad C_{10}=\begin{bmatrix}0&0&0&0&0&0\\ 0&0&0&0&0&0\\ 0&0&0&0&0&0\\ c_{167}&c_{168}&c_{169}&c_{1610}&c_{1611}&c_{1612}\\ c_{177}&c_{178}&c_{179}&c_{1710}&c_{1711}&c_{1712}\\ c_{187}&c_{188}&c_{189}&c_{1810}&c_{1811}&c_{1812}\end{bmatrix} \tag{B.17}$$

$$C_{13}=\begin{bmatrix}c_{191}&c_{192}&c_{193}&c_{194}&c_{195}&c_{196}\\ c_{201}&c_{202}&c_{203}&c_{204}&c_{205}&c_{206}\\ c_{211}&c_{212}&c_{213}&c_{214}&c_{215}&c_{216}\\ c_{221}&c_{222}&c_{223}&c_{224}&c_{225}&c_{226}\\ c_{231}&c_{232}&c_{233}&c_{234}&c_{235}&c_{236}\\ c_{241}&c_{242}&c_{243}&c_{244}&c_{245}&c_{246}\end{bmatrix} \tag{B.18}$$

$$C_3=C_4=C_5=C_6=C_{11}=C_{12}=C_{14}=\mathbf{0}_{(6\times6)}$$

$$C_{15}=\begin{bmatrix}c_{1913}&c_{1914}&c_{1915}&c_{1916}&c_{1917}&c_{1918}\\ c_{2013}&c_{2014}&c_{2015}&c_{2016}&c_{2017}&c_{2018}\\ c_{2113}&c_{2114}&c_{2115}&c_{2116}&c_{2117}&c_{2118}\\ 0&0&0&0&0&0\\ 0&0&0&0&0&0\\ 0&0&0&0&0&0\end{bmatrix};\quad C_{16}=\begin{bmatrix}0&0&0&0&0&0\\ 0&0&0&0&0&0\\ 0&0&0&0&0&0\\ c_{2219}&c_{2220}&c_{2221}&c_{2222}&c_{2223}&c_{2224}\\ c_{2319}&c_{2320}&c_{2321}&c_{2322}&c_{2323}&c_{2324}\\ c_{2419}&c_{2420}&c_{2421}&c_{2422}&c_{2423}&c_{2424}\end{bmatrix} \tag{B.19}$$

in which

$$\begin{gathered}n=1,\ldots,6\\ C_{13n}=[M\omega^2+(0.5.Ml\omega^2-I_{x1}\Omega_3^2)s_n+EI_1s_n^3+iI_{x1}\omega\Omega_3\alpha_n]e^{s_nL_1}\\ C_{14n}=[2Ml\omega^2+(Ml^2\omega^2-4I_{xM}\Omega_3^2+4I_{yM}\omega^2)s_n-4EI_1s_n^2+4i\alpha_n\omega\Omega_3(I_{xM}-I_{yM})]e^{s_nL_1}\\ C_{15n}=[(I_{xM}\omega^2-I_{yM}\Omega_3^2)\alpha_n-GJ_1\alpha_ns_n+i\omega\Omega_3(I_{xM}-I_{yM})s_n]e^{s_nL_1}\\ C_{16n}=[1+0.5ls_n]e^{s_nL_1};\quad C_{17n}=\alpha_ne^{s_nL_1};\quad C_{18n}=s_ne^{s_nL_1}\\ C_{19n}=[1+ls_n]e^{s_nL_1}\quad;\quad C_{20n}=s_ne^{s_nL_1};\quad C_{21n}=\alpha_ne^{s_nL_1}\\ C_{22n}=[1+0.5ls_n]e^{s_nL_1};\quad C_{23n}=\alpha_ne^{s_nL_1};\quad C_{24n}=s_ne^{s_nL_1}\end{gathered} \tag{B.20}$$

$$n=7,\ldots,12\rightarrow c_{16n}=-e^{s_nL_2};\quad c_{17n}=-s_ne^{s_nL_2};\quad c_{18n}=-\alpha_ne^{s_nL_2} \tag{B.21}$$

$$n=13,\ldots,18\rightarrow c_{19n}=-e^{s_nL_3};\quad c_{20n}=s_ne^{s_nL_3};\quad c_{21n}=\alpha_ne^{s_nL_3} \tag{B.22}$$

$$n=19,\ldots,24\rightarrow c_{22n}=-e^{s_nL_4};\quad c_{23n}=s_ne^{s_nL_4};\quad c_{24n}=\alpha_ne^{s_nL_4} \tag{B.23}$$

where s_n are found from Eq. (A.7) and Eq. (A.11)–(A.13).

Finally, in this case the characteristic equation reduces to

$$\det\begin{bmatrix}C_1&C_2&C_3&C_4\\ C_5&C_6&C_7&C_8\\ C_9&C_{10}&C_{11}&C_{12}\\ C_{13}&C_{14}&C_{15}&C_{16}\end{bmatrix}=0 \tag{B.24}$$

References

[1] W. Weaver, S.P. Timoshenko, D.H. Young, *Vibration Problems in Engineering*, Wiley, New York, 1974 (Re-issued 1990).
[2] D.C.D. Oguamanam, Free vibration of beams with finite mass rigid tip load and flexural–torsional coupling, *International Journal of Mechanical Sciences* 45 (2003) 963–979.
[3] H. Salarieh, M. Ghorashi, Free vibration of Timoshenko beam with finite mass rigid tip load and flexural–torsional coupling, *International Journal of Mechanical Sciences* 48 (2006) 763–779.
[4] H. Gokdag, O. Kopmaz, Coupled bending and torsional vibrations of a beam with tip and in-span attachments, *Journal of Sound and Vibration* 287 (2005) 591–610.
[5] M. Esmaeili, N. Jalili, M. Durali, Dynamic modeling and performance evaluation of a vibrating microgyroscope under general support motion, *Journal of Sound and Vibration* 301 (1–2) (2007) 146–164.
[6] V. Bhadbhade, N. Jalili, S.N. Mahmoodi, A novel piezoelectrically actuated flexural/torsional vibrating beam gyroscope, *Journal of Sound and Vibration* 311 (2008) 1305–1324.
[7] M. Esmaeili, M. Durali, N. Jalili, Ring microgyroscope modeling and performance evaluation, *Journal of Vibration and Control* 12 (5) (2006) 537–553.
[8] E. Kanso, A.J. Szeri, A. Pisano, Cross-coupling errors of micromachined gyroscopes, *Journal of Microelectromechanical Systems* 13 (2) (2004) 323–331.
[9] T.K. Tang, R.C. Gutierrez, et al., A packaged silicon MEMS vibratory gyroscope for microspacecraft, Proceedings of IEEE, 10th Micro Electro Mechanical Systems Workshop, Nagoya, Japan, 26–30 January 1997, pp. 500–505.
[10] C.M. Royle, C.H.J. Fox, The mechanics of an oscillatory rate gyroscope with piezoelectric film actuation and sensing, *Proceedings, Institution of Mechanical Engineers, Part C: Journal of Mechanical Engineering Science* 215 (10) (2001) 1211–1221.
[11] V. Bhadbhade, Coupled flexural–torsional vibrations of a cantilever beam gyroscope with application to rocking mass gyroscopes, MS Thesis, Department of Mechanical Engineering, Clemson University, 2006.
[12] M. Dadfarnia, N. Jalili, B. Xian, D.M. Dawson, A Lyapunov-based piezoelectric controller of flexible Cartesian robot manipulators, *ASME Transactions on Journal of Dynamic Systems, Measurement and Control* 126 (2) (2004) 347–358.
[13] M. Dadfarnia, N. Jalili, Z. Liu, D.M. Dawson, an observer-based piezoelectric control of flexible Cartesian robot arms: theory and experiment, *Journal of Control Engineering Practice* 12 (8) (2004) 1041–1053.
[14] R.B. Bhat, S. Chakraverty, *Numerical Analysis in Engineering*, Alpha Science, 2004.